Available online at www.sciencedirect.com
ScienceDirect
Earth and Planetary Science Letters 252 (2006) 107–118
EPSL
www.elsevier.com/locate/epsl

Climate change and Late Pliocene acceleration of erosion in the Himalaya

Katharine W. Huntington [a,*], Ann E. Blythe [b,c], Kip V. Hodges [a,1]

[a] Department of Earth, Atmospheric and Planetary Sciences, Massachusetts Institute of Technology, 77 Massachusetts Ave, MIT 54-1024, Cambridge, MA 02139, USA
[b] Department of Earth Sciences, University of Southern California, Los Angeles, California 90089, USA
[c] Department of Geology, Occidental College, Los Angeles, California 90041, USA

Received 7 March 2006; received in revised form 13 September 2006; accepted 14 September 2006
Available online 1 November 2006
Editor: C.P. Jaupart

Abstract

Studies of active mountain ranges suggest that atmospheric and geodynamic processes may be strongly coupled through erosion — a hypothesis that has led to a debate over the relative importance of climate and far-field tectonic forcing in influencing erosion. We addressed this debate by developing the detailed long-term erosional history of a transect in the central Annapurna Range of Nepal for comparison with the climate and tectonic forcing histories of the region. Patterns of apatite fission-track and muscovite $^{40}Ar/^{39}Ar$ apparent ages with elevation indicate a five-fold increase in apparent erosion rate between 2.5 and 0.9 Ma ago. The time frame for this change corresponds to that of global climate destabilization associated with the onset of Northern Hemisphere glaciation and an intensification of the Asian monsoon. There is no evidence for important changes in the far-field tectonics of the Himalayan–Tibetan orogenic system over that interval, suggesting a largely climatic driver for enhanced erosion at the Himalayan range front.

Keywords: Himalaya; erosion; climate; fission-track geochronology; Argon geochronology

1. Introduction

It has long been recognized that rock deformation and surface processes interact to shape landscapes [1,2]. More recently, both modelling studies [3–6] and field-based studies of active mountain ranges have suggested that atmospheric and geodynamic processes may be strongly coupled through erosion [7–15]. This intriguing hypothesis has led Earth scientists to debate the relative importance of climate and far-field tectonic forcing in influencing erosion over million-year timescales [16].

One way to address this debate is to examine spatial correlations among proxies for climate, exhumation, and deformation [7–15,17]. An example of this approach is the work of Reiners et al. [7], who found that erosional patterns over the past several million years in the North Cascade Mountains, Washington, matched well with precipitation patterns. An alternative tactic is to find a mountainous region

* Corresponding author. Tel.: +1 617 253 5735; fax: +1 617 252 1800.
E-mail addresses: kruhl@mit.edu, katharine.w.huntington@alum.mit.edu (K.W. Huntington).
[1] Present address: School of Earth and Space Exploration, Arizona State University, Tempe, Arizona 85287, USA.

0012-821X/$ - see front matter © 2006 Elsevier B.V. All rights reserved.
doi:10.1016/j.epsl.2006.09.031

where there has been a major change in erosional rate or pattern, determine the timing of this change, and search for temporal correlations with changes in climate or tectonic activity (e.g., a change in convergence rate, or a major reorganization of structural patterns). If one of these forcing factors has changed but the other has not, it is logical to deduce that the one which changed had a major influence on erosion in the studied region. This exercise requires that the timing of the erosion rate change be known precisely, and examples of this are relatively rare in the geologic literature.

In this paper, we report a thermochronologic dataset that provides an unusually sharp definition of the timing of a major acceleration in apparent erosion rate in the central Himalaya. The timing of this acceleration coincides with that of a dramatic destabilization in global climate, providing strong evidence from the bedrock record of a coupling between climate and long-term erosion in the Himalaya.

2. Approach and geologic setting

Muscovite is a common rock-forming mineral in the metamorphic core of the Himalaya and, as a consequence, it figures prominently in thermochronometric studies of the orogen. For cooling rates typical of regionally metamorphosed terrains, a muscovite $^{40}Ar/^{39}Ar$ date represents the time a sample cooled through the ~350 °C closure isotherm [18,19]. Among the most frequently encountered accessory minerals in Himalayan metamorphic rocks is apatite, which is amenable to fission-track dating; at nominal cooling rates, apatite fission-track dates represent cooling

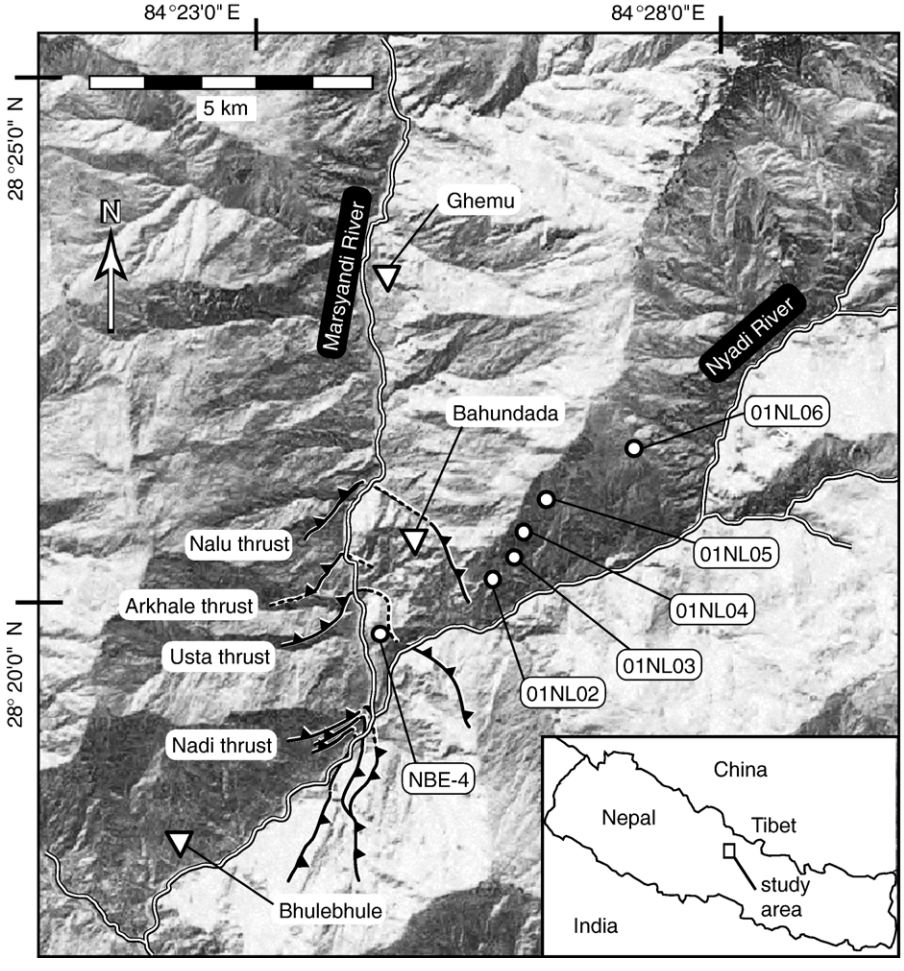

Fig. 1. Simplified structural map of study area on shaded-relief basemap. Map symbols: bedrock sample locations (white circles); from North to South, towns of Ghemu, Bahundada and Bhulebhule (white triangles); structures as mapped by Hodges et al. [8], with black lines with triangles indicating faults, dashed where inferred, from north to south, the Nalu thrust, Arkhale thrust, Usta thrust, and Nadi thrust.

through ~140 °C [20]. If we assume a geothermal gradient during the cooling interval and convert such closure temperature estimates to "closure depths", it is possible to crudely estimate the average rate of erosion from the time of closure to the present by dividing the closure depth by the elapsed time since either a fission-track or $^{40}Ar/^{39}Ar$ date [21].

Fission-track dates for metamorphic rocks of the physiographic Higher Himalaya are typically quite young, in most cases within error of 0 to less than 3 Ma [17,22–24]. Such young dates imply extremely rapid erosional exhumation in the recent past. In contrast, published muscovite $^{40}Ar/^{39}Ar$ ages for most of the Higher Himalaya are Miocene [25–31]. As pointed out by Sorkhabi et al. [23], this difference suggests that the period of rapid erosion recorded by fission-track thermochronometry does not extend far back into the geologic past. Based on a comparison of two $^{40}Ar/^{39}Ar$ detrital mineral thermochronology methods for estimating erosion rates in the Annapurna Range of central Nepal, Ruhl and Hodges [32] suggested that the accelerated erosion hypothesized by Sorkhabi et al. [23] probably began in the Pliocene.

One way to better refine our understanding of the timing of this transition involves the thermochronometry of samples collected along steep topographic profiles. Such datasets provide an opportunity to estimate erosion rates independent of assumptions about the geothermal gradient. (Here we assume that exhumation occurs only via erosion.) During exhumation, samples collected in valleys travel shorter distances from the closure isotherm to the surface than samples collected from ridge tops. Thus, cooling ages increase with elevation at a rate that is proportional to the long-term erosion rate during the closure interval, which we define as the period over which the samples along the transect cooled through the closure isotherm. The inverse of the slope of the best-fit line through an array of age-elevation data therefore can be used as a rough proxy for the average erosion rate over the closure interval [19,33]. Note, however, that non-vertical exhumation pathways and the influence of topography on closure isotherm geometry have the potential to complicate the interpretation of age-elevation gradients in terms of erosion rates [34,35]. This is because the approach of using the slope of the best-fit line through a suite of age-elevation data to infer erosion rates hinges on several assumptions, including: (1) that all samples cooled through the closure isotherm at the same elevation (depth) with respect to some datum, such as sea level, and (2) that all samples followed vertical exhumation paths from the closure isotherm to the surface. In this paper, we compare muscovite $^{40}Ar/^{39}Ar$ and apatite fission-track dates for samples collected along a single age-elevation profile over a lateral distance short enough to largely eliminate problems related to coupled rock and isotherm advection [34]. Moreover, since we are interested in *changes* in apparent erosion rate, rather than absolute rates, problems related to non-vertical exhumation paths are largely unimportant for this exercise. By examining how the age-elevation profiles for the two thermochronometers differ, we were able to explore variations in apparent erosion rates over different parts of the time–temperature history of the same rock column in a simple-minded, yet effective, way. In Section 4 we discuss possible limitations on the

Table 1
Apatite fission-track results and sample locations

Sample	Lat. (E), long. (N)	Elev. (m)	# grains	Standard track density ($\times 10^6$ cm^{-2})	Fossil track density ($\times 10^4$ cm^{-2})	Induced track density ($\times 10^4$ cm^{-2})	Chi square prob. (%)	Central age $\pm 2\sigma$ (Ma)
NBE-4	28° 19.538′ 84° 24.095′	900	See Burbank et al. [17]					1.9±2.2
01NL-02	28° 20.006′, 84° 25.274′	1400	40	1.51	6.6 (14)	2889 (6140)	41	0.6±0.4
01NL-03	28° 20.228′, 84° 25.489′	1695	28	1.47	5.9 (9)	3312 (5066)	96	0.5±0.4
01NL-04	28° 20.430′ 84° 25.588′	1981	30	1.47	6.8 (10)	2314 (3421)	84	0.8±0.4
01NL-05	28° 20.721′ 84° 25.816′	2314	40	1.67	7.4 (15)	2518 (5109)	82	0.9±0.4
01NL-06	28° 21.165′ 84° 26.288′	2697	10	1.62	8.6 (4)	3256 (1521)	53	0.8±0.8

Number of tracks counted in parentheses.

robustness of our conclusions due to the effects of topography and non-vertical exhumation.

Samples were collected along a steep ridge separating the Marsyandi and the Nyadi rivers of the Annnapurna Range of central Nepal (Fig. 1). They include pelitic gneisses of the Neoproterozoic Greater Himalayan sequence, as well as structurally underlying pelitic schists and phyllites of the lower part of the Meso–Paleoproterozoic Lesser Himalayan sequence [8,30,36]. The lowest sample comes from near the level of the Marsyandi–Nyadi confluence, the highest is from a point nearly 1800 m above, and the transect spans a horizontal distance of ~4.6 km. Muscovite $^{40}Ar/^{39}Ar$ dates for these samples were determined as part of an evaluation of the fidelity of detrital muscovite thermochronology in the Nyadi catchment [37]; they are reviewed here for comparative purposes. The apatite fission-track date for the lowest of these samples was published previously by Burbank et al. [17]. We present here for the first time the apatite fission-track dates for all other samples from the transect.

3. Fission-track analytical methods

Aliquots rich in apatite were prepared from each sample by Donelick Analytical using standard magnetic and gravimetric techniques. Final separates for analyses were hand-picked to ensure purity. The apatites were mounted in epoxy, and their surfaces ground and polished. The mounts were etched in 7% HNO_3 at 18 °C for 22 s. An "external detector" (e.g., [38]), consisting of low-U (<5 ppb) Brazil Ruby muscovite, was used for each sample. Samples were irradiated in the Cornell University and Oregon State TRIGA nuclear reactors. Following irradiation, the Brazil Ruby muscovites were etched in 48% HF at 18 °C for 30 min. Tracks in crystals with well-etched, clearly visible tracks and sharp polishing scratches were counted using a 100X dry lens and 1250X total magnification. A Kinitek stage and software written by Dumitru [39] were used for analyses. Parentheses in Table 1, where the results are summarized, show the number of tracks counted. Standard and induced track densities were determined on external detectors (with a geometry factor of 0.5), and fossil track densities were determined on internal mineral surfaces. Ages were calculated using $\zeta = 359 \pm 10$ for dosimeter glass CN5 (e.g., [40]). All ages are central ages, with the conventional method [41] used to determine errors on sample ages. The χ^2 test was used to judge the probability that individual grain ages for each sample belong to a single population with a Poisson distribution [42]. All ages were calculated using TrackKey [43].

4. Results and interpretations

The lowest elevation sample plotted in Fig. 2 yielded anomalous results; the significance of this is discussed below. The remaining samples, collected at elevations ranging from 1400 to 2697 m, contributed apatite fission-track and muscovite $^{40}Ar/^{39}Ar$ data that are indicative of simple exhumation through the ~140 °C and ~350 °C closure isotherms, respectively. The muscovite dates for these samples range from 2.46±0.22 Ma to 5.10±0.23 Ma [37], and are strongly correlated with elevation; the Pearson correlation coefficient for these data is 0.99. A least-squares linear regression routine – weighing the analytical uncertainty on the sample dates as the dependent variable [44] – predicts an increase in muscovite $^{40}Ar/^{39}Ar$ date of roughly 1 Ma for every 0.57 km of elevation gain, equivalent to an apparent erosion rate of 0.57 km/My (or mm/yr). More importantly, the linearity of the plot of elevation vs. $^{40}Ar/^{39}Ar$ date implies a more or less uniform erosion rate between 5.1 and 2.5 Ma. Detrital muscovite $^{40}Ar/^{39}Ar$ cooling ages ranging from ~2.5 to ~11 Ma correlate well with hypsometry in the Nyadi catchment [32]. This suggests that the period of uniform erosion at a rate of roughly 0.57 km/My recorded

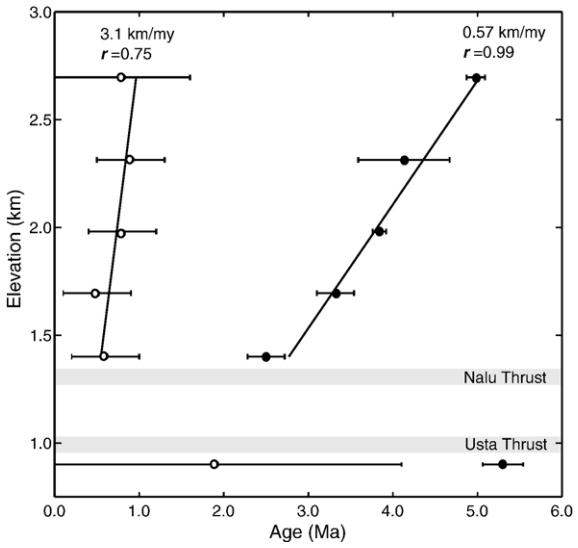

Fig. 2. Cooling age vs. sample elevation. Cooling age and 2σ uncertainty vs. sample elevation plotted with least-squares regression best-fit age-elevation gradient for apatite fission-track data (open circles) and muscovite $^{40}Ar/^{39}Ar$ data (black circles).

by the bedrock muscovite samples extended well into the Miocene [37].

Apatite fission-track dates for these samples range from 0.5±0.4 Ma to 0.9±0.4 Ma (Table 1). The relatively large errors, reported at the 2σ or ~95% confidence level, can be attributed to the very small numbers of fission-tracks in these young apatites. Nevertheless, the age variation is reasonably well correlated with elevation (Fig. 2); the Pearson correlation coefficient (r) for these data is 0.75. A linear fit to the data, produced in the same way as the fit for the $^{40}Ar/^{39}Ar$ data, predicts an increase in apatite fission-track age of 1 Ma for every 3.1 km of elevation gain. Monte Carlo simulations indicate that the roughly five-fold difference between the apatite and muscovite age-elevation gradients is statistically significant despite the relatively large uncertainties in the apatite data (see Appendix A). This conclusion is bolstered by the simple observation that the 1400 m sample was at a temperature of ~350 °C as recently as 2.5 Ma and is now exposed at the surface. Without invoking an unrealistically high geothermal gradient (~245 °C/km), it is not possible to explain how a sample could have cooled this rapidly if exhumation continued at a constant rate of 0.57 km/My from 2.5 Ma to the present.

Whether or not the apparent erosion rates of 3.1 km/My for the fission-track data and 0.57 km/Ma for the $^{40}Ar/^{39}Ar$ data can be taken as actual measures of the erosion rate averaged over the 0.5–0.9 Ma and 5.1–2.5 Ma intervals, respectively, depends on the kinematics of exhumation and the topography during the closure intervals, and the (possibly dynamic) morphology of the closure isotherms at depth [34,35,45–48].

While closure isotherms for low-temperature thermochronometers may be significantly perturbed by topography when erosion is rapid and relief is high, closure isotherms for higher-temperature thermochronometers such as the $^{40}Ar/^{40}Ar$ muscovite system (closure temperature, T_C ~350 °C) are relatively insensitive to topographic effects and remain approximately horizontal over a wide range of erosion rates and topographic settings (e.g., [46]). As a result, under some circumstances a difference in apparent erosion rates from age-elevation gradients corresponding to different closure temperatures could be explained not by a change in erosion rate, by simply as the result of topographic effects (e.g., Fig. 2 in [48]).

In order to investigate these potential complications, we used the finite-element program FRACTure [49,50] to calculate the three-dimensional thermal field for the region of mountainous topography surrounding our study area. We then tracked the thermal histories of rock particles as they were exhumed through this thermal field and predicted apatite fission-track and muscovite $^{40}Ar/^{40}Ar$ cooling ages sampled at the surface using the program TERRA [51] in an approach similar to that of Ehlers et al. [52] and Whipp et al. [58]. The model is described in Appendix B, and age-elevation gradient results are summarized in Table 1. If we assume, for simplicity, purely vertical exhumation at a rate of 0.50 km/My, the model predicts a muscovite age-elevation gradient of 0.59 km/My (consistent with the data obtained by Huntington and Hodges [37]) and an only slightly higher apatite age-elevation gradient of 0.63 km/My. Following the statistical approach outlined in Appendix A, it can be shown that the probability of this gradient being indistinguishable from the observed gradient of 3.1 km/My, even given the magnitude of the errors for the apatite data, is less than 1 in 10,000. These results indicate that if samples follow vertical exhumation pathways to the surface, no single constant erosion rate can explain both the muscovite and apatite data.

But can a single constant erosion rate account for the difference in muscovite and apatite age-elevation gradients if non-vertical exhumation pathways are considered? Several models for the Pliocene to Holocene transport of Higher Himalayan rocks have been proposed that predict exhumation pathways with a significant component of lateral motion [8,54–57]. As lateral transport changes the distance rocks travel from the closure isotherm to the surface and crustal-scale faults may be expected to perturb the position of the closure isotherms with respect to exhumation trajectories, lateral rock transport and structural discontinuities may result in age-elevation gradients that do not reflect long-term erosion rates. In order to quantify the potential magnitude of these effects and to determine if they are likely to account for the observed difference in muscovite and apatite age-elevation gradients, we also calculated apparent erosion rates from predicted muscovite and apatite age-elevation gradients for simulations with lateral transport and thrust geometries (Appendix B, Table 2). When these non-vertical exhumation pathways are considered (true model erosion rates of 0.5–3.0 km/My), apatite and muscovite age-elevation gradients vary by <33% in all cases (Table 2). This difference is still less than half of the difference (82%) we observe in the Nyadi data, suggesting that a single constant erosion rate cannot satisfy the data even when lateral transport is considered.

Table 2
Age-elevation predictions for the Nyadi Transect from thermal-kinematic model results

Observed	AFT (km/My)	MAr (km/My)	Difference (%)
	3.10	0.57	82
Vertical model rate v_z (km/My)	AFT vertical	MAr vertical	Difference (%)
0.5	0.63	0.59	6
1.0	1.29	1.22	5
2.0	2.70	2.58	4
2.5	3.43	3.28	4
3.0	4.20	3.97	5
Lateral model rate v_z (km/My)	AFT lateral	MAr lateral	Difference (%)
0.5	0.65	0.55	15
1.0	1.40	1.09	22
3.0	5.36	4.59	14
Thrust model rate v_z (km/My)	AFT thrust	MAr thrust	Difference (%)
0.5	0.63	0.52	17
1.0	1.33	1.08	19
3.0	5.16	3.44	33

"Observed" indicates results of actual measurements from the Nyadi transect from this study and [37]. The designations "vertical," "lateral" and "thrust" indicate results for model simulations (see Appendix B for model details). The model rate (v_z) is the vertical particle velocity prescribed in the model, and is equal to the vertical component of the erosion rate. Particle trajectories are vertical in the "vertical" model simulation, and the "lateral" and "thrust" geometries prescribe particle paths that have a significant component of horizontal transport. AFT indicates age-elevation gradient for apatite fission-track samples, and MAr indicates age-elevation gradient for muscovite $^{40}Ar/^{39}Ar$ samples. Difference % is the percent difference between age-elevation gradients for the muscovite and apatite sample transects, and is calculated as (AFT − MAr) / AFT * 100.

Three-dimensional modeling of this sort allows us to rule out likely erosional scenarios that do not involve a rate change. In addition to the modeling results presented here, more comprehensive work by Whipp et al. [58] indicates a rate acceleration prior to the time spanned by the apatite fission-track dates. However, our approach and that employed by Whipp et al. cannot be used to pinpoint the exact rates before and after this change because the models simulate steady-state erosion and because predicted age-elevation gradients are sensitive to the kinematics of deformation during exhumation (Table 1, [35]). In this part of the Himalaya, however, there is no structural evidence to suggest that there were major variations in deformation kinematics in this region over the past 5–6 Ma [31,59]. Thus, the roughly five-fold difference between the fission-track and $^{40}Ar/^{39}Ar$ exhumation rates is important regardless of whether or not the apparent rates are equivalent to the actual rates. More importantly, the data strongly imply that the acceleration in erosion rate occurred sometime between ~2.5 and ~0.9 Ma.

Ruhl and Hodges [32] noted that detrital muscovite $^{40}Ar/^{39}Ar$ cooling ages from the Nyadi catchment are well correlated with hypsometry, implying that the modern catchment is eroding uniformly. Along with the data presented here, this observation suggests that the timescale for relief adjustment to accelerated exhumation must be on the order of ~0.9–2.5 Ma. This is consistent, to first order, with the response time that would be predicted based on the expected rate of vertical knickpoint migration through the Nyadi catchment. Niemann et al. [60] pointed out that when uplift rate varies temporally, knickpoints travel through a catchment with constant vertical velocity, and the response time of a catchment to a change in rate follows directly from the vertical velocity of the knickpoint. If incision depends on unit stream power [61] and channel concavity does not vary with uplift rate, this response time should be given by the ratio of the modern topographic relief (~6 km) to the final erosion rate (~3.1 km/My).

5. Corroborating evidence for a 2.5–0.9 Ma change in erosion rate in the central Himalaya

In addition to the work described here, three other geochronologic studies in the Himalaya appear to support a regional Late Pliocene–Pleistocene increase in erosion rate.

The first is a study in press by Blythe et al. [62] aimed at substantially expanding the database of thermochronologic dates in the Marsyandi drainage surrounding our field site with additional fission-track and (U–Th)/He analyses. While the data of Blythe and co-workers alone do not require a rate change, they are consistent with a Late Pliocene–Pleistocene erosion rate acceleration for the central Annapurna Range, as indicated by the thermo-kinematic modeling of Whipp et al. [58].

The second study, published only in abstract form [22], found that apatite fission-track dates for samples collected on a climbing expedition to Mount Everest on the Nepal–Tibet border (~27°59′ N; 86°56′ E) ranged systematically from 1.7±1.4 Ma to 7.1±1.2 Ma as a function of elevation between 2560 and 6500 m. The authors reported a small increase in age with elevation below 4000–5000 m and a much larger increase at higher elevations. When such inflections are observed in age-elevation profiles, they are usually interpreted as an indication of a pulse of exhumation beginning

approximately at the time of closure of the samples that define the inflection [63]; in the case of the Everest dataset, the inflection implies an exhumation rate increase at ~2–3 Ma.

A second example of such an inflection can be found by comparing data from two apatite fission-track studies of different lobes of the Badrinath–Gangotri plutonic complex in the Garhwal Himalaya of India. Working on samples collected along the Bhagirathi River at ~31°00′ N; 79°00′ E and at elevations ranging from 3020–4370 m, Sorkhabi et al. [23] documented an increase in apparent age from 1.5±0.6 Ma to 2.4±0.5 Ma. These data indicate a gradient of ~2.5 km/My, which is similar to our Marsyandi apatite fission-track gradient. However, Searle et al. [64] reported a much shallower gradient (~0.4 km/My) for samples collected from the 5000–5500 m levels of the Shivling massif (~33°23′ N; 76°27′ E), ranging in age from 2.2 to 3.5 Ma. The youngest of the Shivling ages (2.2±0.4 Ma) overlaps with the oldest ages recovered by Sorkhabi and co-workers, indicating the approximate time of accelerated unroofing.

The expanded thermochronologic database of Blythe et al. [62] strongly suggests that the results presented in this paper for a single sample transect are characteristic of the central Annapurna Range as a whole. In addition, while the Everest data have not been completely published and neither they nor the Badrinath–Gangotri data are as compelling as the Marsyandi data, we regard it as significant that elevation-age patterns from widely separated locations in the Himalaya can be interpreted easily in terms of a sharp increase in exhumation rate between ~2.5 and 0.9 Ma.

6. Arguments in favor of climate change as the cause of accelerated erosion

Was the abrupt increase in exhumation rate between 2.5 and 0.9 Ma documented here caused by climate change, a change in the pattern and rate of far-field tectonic forcing, or both? We would argue that the evidence points to a predominantly climatic driver. Although there was a rapid change in the surface pattern of tectonic activity in the Himalayan hinterland over the Middle to Late Miocene interval, the period between ~5 Ma and ~1 Ma was marked by gradual and passive uplift of the Greater Himalayan sequence relative to the downgoing Indian plate [65]. In contrast, the Late Pliocene–Pleistocene interval was one of profound climate change on a global scale. Although there is some debate regarding the exact timing of the onset of Northern Hemisphere glaciation, virtually all available data point to at least a dramatic intensification of it between ~3.0 and ~2.4 Ma [66,67]. At the same time, an increase in the frequency and amplitude of oscillations in the $\delta^{18}O$ in signatures of benthic foraminifera indicate a marked destabilization of global climate [68,69]. In Asia, the effects of this included an intensification of the East Asian winter monsoon and establishment of the current seasonal pattern of the Indian "summer" monsoon [70–72]. Although some workers have argued against it [73,74], many argue that Late Pliocene–Pleistocene climate destabilization corresponded with a dramatic increase in sedimentation rates in basins surrounding the Himalayan–Tibetan orogenic system [75,76]. Given the lack of geologic evidence for tectonic forcing of a ~2.5–0.9 Ma increase in exhumation rate in the Higher Himalaya, our data support arguments for climatic forcing of global increases in Late Pliocene–Pleistocene sediment accumulation rates [69,77].

7. Evidence for late-stage slip near the trace of the Main Central thrust

Although there is no evidence for a change in far-field tectonic forcing in the Himalaya over the past 2.5 Ma, recent studies have revealed evidence for very recent out-of-sequence faulting along the Himalayan range front [8,11,78]. Our findings provide additional support for these observations. The thermochronometric data for samples collected between 1400 m and 2697 m are consistent with simple exhumation through the closure-temperature isotherms for the apatite fission-track and muscovite $^{40}Ar/^{39}Ar$ systems. That is, the approximately linear age-elevation relationships suggest that (1) the samples were exhumed together as a block; (2) the rate was constant during the closure interval for muscovite (i.e., during the time period represented by the sample ages, from 5.1 to 2.5 Ma); and (3) the rate was roughly constant again during the closure interval for apatite (i.e., during the time period represented by the sample ages, from ~0.9 to ~0.5 Ma). However, neither the apatite fission-track date nor the muscovite $^{40}Ar/^{39}Ar$ date for the lowest elevation (900 m) sample in our profile falls on the simple age-elevation trends exhibited by the other samples. Having only the muscovite $^{40}Ar/^{39}Ar$ dates at their disposal, Huntington and Hodges [37] suggested that the disruption in that trend could have been caused by post-2.46 Ma fault activity. Indeed, the 900 m sample was separated from the other samples by two faults. The structurally highest of these is the Nalu thrust [8]. Separating gneisses of the Greater Himalayan sequence in the hanging wall from

Lesser Himalayan sequence footwall rocks with a distinctive metamorphic history [30], this structure corresponds to the Main Central Thrust as traditionally defined in Nepal by a variety of workers [36,79,80]. The other fault separating the inconsistent sample from the rest of the transect is the Usta Thrust [8]. Martin et al. [81] recently suggested that this is the actual Main Central Thrust on the basis of a contrast across it in detrital U–Pb zircon ages and Nd isotopic characteristics. Regardless of which interpretation of the position of the Main Central Thrust is correct, the muscovite $^{40}Ar/^{39}Ar$ data suggest that there has been significant thrust-sense displacement on the Nalu thrust, Usta thrust, or both. The new apatite data presented here – which show the same relative offset of the age-elevation trend as the $^{40}Ar/^{40}Ar$ data – provide important corroborating evidence for young displacement. Moreover, the apatite data provide better constraints on the age of the latest post-Pliocene displacement, requiring that it be younger than ~1 Ma.

8. Discussion and conclusions

The significantly different age-elevation gradients defined by apatite fission-track and muscovite $^{40}Ar/^{39}Ar$ bedrock data provide strong evidence that a substantial erosion rate acceleration began between ~2.5 and 0.9 Ma. Although the apatite fission-track and muscovite $^{40}Ar/^{39}Ar$ thermochronometers constrain the timing of this transition reasonably well, we note that it may be possible to pinpoint it even more precisely using a thermochronometer that is sensitive to temperatures between ~140 and ~350 °C if analytical uncertainties are small. For example, we would predict that the zircon (U–Th)/He thermochronometer, sensitive to a temperature of roughly 200 °C for nominal cooling rates [82], would exhibit a kinked age-elevation profile near the Marsyandi–Nyadi confluence with the point of inflection located between 2.5 and 0.9 Ma.

We are not aware of any evidence for a significant change in far-field tectonic forcing during the ~2.5–0.9 Ma timeframe; however, there exists a wealth of evidence for global-scale climate change at approximately the time of this change in exhumation rate. As a consequence, we conclude that climate more likely had the stronger influence on enhancing long-term erosion and exhumation at the Himalayan range front during Late Cenozoic time. While it is impossible to prove causation from correlation, it could be argued that a temporal correlation of climate change and erosion rate change provides much stronger evidence for a causal relationship between climate and erosion than a spatial correlation of precipitation and exhumation patterns (cf., [7]). It is difficult to disprove the null hypothesis that enhanced precipitation coincides with steps in topography associated with high exhumation rates simply due to the physics of weather, even in the absence of a causal relationship between climatic forcing and erosion. However, there is no physical reason to expect a change in exhumation to occur in concert with climate change unless the two are coupled.

Information regarding the timescales of landscape adjustment to climate perturbations may help us to evaluate the strength of these relationships. In the case of the Nyadi catchment, a series of special circumstances allows us to place bounds on the landscape response time to this change in climate forcing: we have constrained the timing of erosion-rate change, and the good correlation of detrital muscovite $^{40}Ar/^{39}Ar$ cooling ages and hypsometry in the Nyadi catchment indicate that modern erosion is uniform. These constraints indicate that relief and channel-profile adjustment to this increase in exhumation rate must have occurred within a time period of roughly 0.9–2.5 Ma, on the order of the response time predicted by knickpoint celerity estimates. A record of this transition may also be expected in the shape of detrital mineral cooling-age distributions from proximal ancient sedimentary deposits, for example in nearby fluvial terraces.

Acknowledgements

We thank D. Whipp and T. Ehlers for their contributions to the thermal modeling component of this work, K. Whipple, Ehlers, A. Heimsath, D. Burbank, P. Reiners, L. Bollinger, and an anonymous reviewer for comments that improved earlier versions of the manuscript, and K. Schmidt for field assistance. Funding was provided by the National Science Foundation Continental Dynamics program for the project entitled "Geomorphic–Geodynamic Coupling at the Orogen Scale".

Appendix A. Statistical comparison of apatite fission-track and muscovite $^{40}Ar/^{39}Ar$ age-elevation gradients

In order to evaluate the significance of the difference between the age-elevation gradients defined by the apatite fission-track and muscovite $^{40}Ar/^{39}Ar$ data, we determined the probability that the two datasets define the same slope using a Monte Carlo approach. For each analyzed apatite fission-track date X_n with one-sigma analytical uncertainty σ_n, we created a random

distribution R_n of 10,000 normally distributed values with a mean equal to X_n and a standard deviation of σ_n. One value was randomly chosen from each of the distributions R_n, and these values were regressed (using the same approach as for the original age-elevation gradient calculations) in order to calculate a slope. This exercise was repeated 10,000 times to produce an array of 10,000 slopes, and each slope was compared with the slope defined by the muscovite $^{40}Ar/^{39}Ar$ data (0.57± 0.048 km/My at the two-sigma confidence level). If the calculated slope was within 2σ error of 0.57, we concluded that the test slope was indistinguishable from the muscovite $^{40}Ar/^{39}Ar$ slope; if it was not, we concluded that the slopes were distinguishable. The percentage of test slopes that were "indistinguishable" provides an excellent empirical indication of the distinctiveness of the actual $^{40}Ar/^{39}Ar$ and fission-track age-elevation gradients. Specifically, the simulations showed that there is less than a 1:10,000 chance that the gradient recorded by the apatite data is equal to the gradient recorded by the muscovite $^{40}Ar/^{39}Ar$ data.

Appendix B. Thermal model details

Our modelling approach is nearly identical to that of Ehlers et al. [1] and Whipp et al. [2]. It consists of three components: a kinematic model, a thermal finite-element model, and a thermochronometer age-prediction model. The kinematic model prescribes the velocity field for nodal advection for the thermal model, and the thermochronometer age-prediction model predicts sample ages at the surface based on their thermal histories as they are exhumed from depth.

Heat transfer occurs as a function of the exhumation geometries given by the kinematic model. In this model, material is assumed to be incompressible and mass is conserved. The topography is prescribed by a 250-m digital elevation model of the study region (size: 140×84 km), and remains static. As a result, the vertical component of the erosion rate at the surface is equal to the vertical component of velocity in the kinematic model (v_z). While the topography varies in three-dimensions, the kinematic field is one-dimensional for the "vertical" model simulations and two-dimensional for the "lateral" and "thrust" simulations. In the "vertical" model simulations, particle paths are vertical.

In the "lateral" model simulations, particles are transported horizontally as they are exhumed. No structural discontinuity is included in the lateral model simulations. For these models, the horizontal velocity v_y is a function of the prescribed vertical component of the erosion rate v_z and the dip of the particle trajectory, which we hold constant at 28° [3]:

$$v_y = \left| \frac{v_z}{\tan(28°)} \right| \tag{1}$$

In the "thrust" model simulations, particles are transported horizontally as they are exhumed along a single, discrete, crustal-scale thrust fault. The fault trace in the thrust simulations intersects with the model topography at the position of the principal thrust of the Main Central Thrust where it has been mapped in the Marsyandi Valley [4]. The fault is simulated as a planar surface composed of two segments — a horizontal segment (dip angle $\Theta=0°$) at 28 km depth and a ramp segment ($\Theta=28°$). Slip occurs parallel to these planes, and the slip rate on the fault is a function of the dip angle and the horizontal convergence velocity across the fault, $v_{converge}$:

$$v_{slip} = \frac{|v_{converge}|}{\cos\theta_i} \tag{2}$$

where Θ_i is the dip of the ith fault segment. The underthrusting rate is set to equal half of $v_{converge}$. For the thrust models, we only predict hanging-wall sample ages. The sample locations for which ages are predicted in the model are located at approximately the same coordinates as the thermochronologic samples that were analyzed in this study. The horizontal transport velocity v_y for these particles is equal to $v_{converge}/2$, and their vertical exhumation rate $v_z(x,y,z)$ is given by

$$v_z(x,y,z) = v_y \cdot \tan\theta_i \tag{3}$$

We calculated the 3D thermal field beneath the model topography to 50 km depth using the steady-state advection–diffusion equation

$$\frac{\nabla(K\nabla T)}{\rho c} - \bar{v}\nabla T = -\frac{A}{\rho c} \tag{4}$$

where T is temperature and $\bar{v}$ is the material velocity from the kinematic model. K, A, ρ, and c are the thermal conductivity, radiogenic heat production per unit volume, density, and heat capacity, respectively. This calculation was performed in the Eulerian reference frame using the finite-element program FRACTure [5,6]. The upper surface has a constant temperature boundary condition (14 °C–7 °C/km elevation above sea level). The constant temperature boundary condition

at the base of the model (50 km depth beneath the average topography) was set to 600 °C. Velocity-dependent shear heating on the fault planes is included after the methods of [7] and Hansen and Carter [8] and with the following assumptions: the fault zone is 1 km wide, the strain rate is equal to the fault slip rate, the maximum allowed shear stress is 50 MPa, and the shear stress is calculated using a brittle pressure-dependent law or ductile temperature-dependent power law, whichever is smaller. Additional heat produced is added to the nodal radiogenic heat production within the shear zone. We also assume that heat transfer by fluid flow is not a major thermal influence.

Thermochronometer ages for the Nyadi transect sample locations are calculated using model-predicted cooling histories, which are calculated by tracking samples from the surface back to different depths in the model. Predicted apatite fission-track ages were calculated using the method outlined by Ehlers et al. [9], and muscovite $^{40}Ar/^{39}Ar$ ages were calculated assuming a closure temperature of 350 °C.

Free parameters in the model include the basal and surface boundary conditions, radiogenic heat production, thermal conductivity, specific heat, density, and kinematic field. We hold constant the boundary condition (600 °C), radiogenic heat production (0.5 $\mu W/m^3$), thermal conductivity (2.5 W/mK), specific heat (800 J/kgK), and density (2750 kg/m^3), and vary the exhumation geometry and rate (0.5–3.0 mm/yr or km/My).

References

[1] W.M. Davis, Bearing of physiography on uniformitarianism, Geol. Soc. Amer. Bull. 7 (1896) 8–11.

[2] G.K. Gilbert, A.P. Brigham, An Introduction to Physical Geography, Appleton, New York, 1911.

[3] K.V. Hodges, J.M. Hurtado, K.X. Whipple, Southward extrusion of Tibetan crust and its effect on Himalayan tectonics, Tectonics 20 (2001) 799–809.

[4] C. Beaumont, R.A. Jamieson, M.H. Nguyen, B. Lee, Himalayan tectonics explained by extrusion of a low-viscosity crustal channel coupled to focused surface denudation, Nature 414 (2001) 738–742.

[5] P.O. Koons, The topographic evolution of collisional mountain belts: a numerical look at the Southern Alps, New Zealand, Am. J. Sci. 289 (1989) 1041–1069.

[6] S.D. Willett, Orogeny and orography: the effects of erosion on the structure of mountain belts, J. Geophys. Res. 104 (1999) 28957–28981.

[7] P.W. Reiners, T.A. Ehlers, S.G. Mitchell, D.R. Montgomery, Coupled spatial variations in precipitation and long-term erosion rates across the Washington Cascades, Nature 426 (2003) 645–647.

[8] K. Hodges, C. Wobus, K. Ruhl, T. Schildgen, K. Whipple, Quaternary deformation, river steepening, and heavy precipitation at the front of the Higher Himalayan ranges, Earth Planet. Sci. Lett. 220 (2004) 379–389.

[9] J.C. Vannay, B. Grasemann, M. Rahn, W. Frank, A. Carter, V. Baudraz, M. Cosca, Miocene to Holocene exhumation of metamorphic crustal wedges in the NW Himalaya: evidence for tectonic extrusion coupled to fluvial erosion, Tectonics 23 (2004).

[10] C.W. Wobus, K.V. Hodges, K.X. Whipple, Has focused denudation sustained active thrusting at the Himalayan topographic front? Geology 31 (2003) 861–864.

[11] C. Wobus, A. Heimsath, K. Whipple, K. Hodges, Active out-of-sequence thrust faulting in the central Nepalese Himalaya, Nature 434 (2005) 1008–1011.

[12] S. Dadson, N. Hovius, H. Chen, W.B. Dade, M.-L. Hsieh, S. Willett, J.-C. Hu, M.-L. Horng, M.-C. Chen, C. Stark, D. Lague, J.-C. Lin, Links between erosion, runoff variability and seismicity in the Taiwan orogen, Nature 426 (2003) 648–651.

[13] R.C. Thiede, B. Bookhagen, J.R. Arrowsmith, E. Sobel, M. Strecker, Climatic control on rapid exhumation along the Southern Himalayan front, Earth Planet. Sci. Lett. 222 (2004) 791–806.

[14] D. Finlayson, D. Montgomery, B. Hallet, Spatial coincidence of rapid inferred erosion with young metamorphic massifs in the Himalayas, Geology 30 (3) (2002) 219–222.

[15] D. Montgomery, G. Balco, S. Willett, Climate, tectonics, and the morphology of the Andes, Geology 29 (7) (2001) 579–582.

[16] P. Molnar, Nature, nurture and landscape, Nature 426 (2003) 612–614.

[17] D.W. Burbank, A.E. Blythe, J.K. Putkonen, B.A. Pratt-Sitaula, E.J. Gabet, M.E. Oskin, A.P. Barros, T.P. Ojha, Decoupling of erosion and precipitation in the Himalaya, Nature 426 (2003) 652–655.

[18] I. McDougall, T.M. Harrison, Geochronology and Thermochronology by the 40Ar/39Ar Method, Oxford University Press, New York, 1998, 261 pp.

[19] K.V. Hodges, Geochronology and thermochronology in orogenic systems, in: R.L. Rudnick (Ed.), The Crust, Treatise on Geochemistry, vol. 3, Elsevier Science, Amsterdam, 2003, pp. 263–292.

[20] G.M. Laslett, P.F. Green, I.R. Duddy, A.J.W. Gleadow, Thermal annealing of fission tracks in apatite, Chem. Geol., Isot. Geosci. Sect. 65 (1) (1987) 1–13.

[21] G.A. Wagner, G.M. Reimer, E. Jäger, Cooling ages derived by apatite fission track, mica Rb–Sr, and K–Ar dating: the uplift and cooling history of the Central Alps, Mem. Univ. Padova 30 (1977) 1–27.

[22] S.C. Bergman, D.Q. Coffield, R. Donelick, J. Corrigan, J. Talbot, P. Cerveny, S. Kelley, Late Cenozoic compressional and extensional cooling and exhumation of the Qomolangma (Mt. Everest) region, Nepal, Abstr. Programs - Geol. Soc. Am. 25 (1993) 176.

[23] R.B. Sorkhabi, E. Stump, K.A. Foland, A.K. Jain, Fission-track and 40Ar/39Ar evidence for episodic denudation of the Gangotri granites in the Garhwal Higher Himalaya, India, Tectonophysics 260 (1997) 187–199.

[24] K. Arita, Y. Ganzawa, Thrust tectonics and uplift processes of the Nepal Himalaya revealed from fission-track ages, J. Geogr. (Jpn.) 106 (1997) 156–167.

[25] K.V. Hodges, Tectonics of the Himalaya and southern Tibet from two perspectives, Geol. Soc. Amer. Bull. 112 (2000) 324–350.

[26] P. Copeland, T.M. Harrison, K.V. Hodges, P. Maruéjol, P. LeFort, A. Pêcher, An Early Pliocene thermal disturbance of the Main Central Thrust, central Nepal: implications for Himalayan tectonics, J. Geophys. Res. 96 (1991) 8475–8500.

[27] A. Macfarlane, K.V. Hodges, D. Lux, A structural analysis of the Main Central thrust zone, Langtang National Park, central Nepal Himalaya, Geol. Soc. Amer. Bull. 104 (1992) 1389–1402.
[28] A.M. Macfarlane, The chronology of tectonic events in the crystalline core of the Himalayas, Langtang National Park, central Nepal, Tectonics 12 (1993) 1004–1025.
[29] R.M. Edwards, 40Ar/39Ar geochronology of the Main Central thrust (MCT) region: evidence for Late Miocene to Pliocene disturbances along the MCT, Marsyangdi River valley, west-central Nepal Himalaya, J. Nepal Geol. Soc. 10 (1995) 41–46.
[30] E.J. Catlos, T.M. Harrison, M.J. Kohn, M. Grove, F.J. Ryerson, C.E. Manning, B.N. Upreti, Geochronologic and thermobarometric constraints on the evolution of the Main Central Thrust, central Nepalese Himalaya, J. Geophys. Res. 106 (2001) 16177–16204.
[31] L. Bollinger, J.P. Avouac, O. Beyssac, E.J. Catlos, T.M. Harrison, M. Grove, B. Goffe, S. S., Thermal structure and exhumation history of the Lesser Himalaya in central Nepal, Tectonics 23 (2004).
[32] K. Ruhl, K. Hodges, The use of detrital mineral cooling ages to evaluate steady-state assumptions in active orogens: an example from the central Nepalese Himalaya, Tectonics 24 (2005) TC4015.
[33] G.A. Wagner, G.M. Reimer, Fission track tectonics: the tectonic interpretation of fission track apatite ages, Earth Planet. Sci. Lett. 14 (1972) 263–268.
[34] J. Braun, Quantitative constraints on the rate of landform evolution derived from low-temperature thermochronology, Rev. Mineral. Geochem. 58 (2005) 351–374.
[35] T.A. Ehlers, Crustal thermal processes and the interpretation of thermochronometer data, Rev. Mineral. Geochem., vol. 58, 2005, pp. 315–350.
[36] M.E. Coleman, U–Pb constraints on Oligocene–Miocene deformation and anatexis within the central Himalaya, Marsyandi valley, Nepal, Am. J. Sci. 298 (7) (1998) 553–571.
[37] K.W. Huntington, K.V. Hodges, A comparative study of detrital mineral and bedrock age-elevation methods for estimating erosion rates, J. Geophys. Res. 111 (2006) F03011, doi:10.1029/2005JF000454.
[38] C.W. Naeser, Fission-track dating and geologic annealing of fission tracks, in: E. Jäger, J.C. Hunziker (Eds.), Lectures in Isotope Geology, Springer-Verlag, Berlin, 1979, pp. 154–169.
[39] T. Dumitru, A new computer automated microscope stage system for fission-track analysis, Nucl. Tracks Radiat. Meas. 21 (1993) 575–580.
[40] A. Hurford, P. Green, The age calibration of fission-track dating, Isot. Geosci. 1 (1983) 285–317.
[41] P. Green, "Track-in-track" length measurements in annealed apatites, Nucl. Tracks 5 (1981) 121–128.
[42] R. Galbraith, On statistical methods for fission track counts, Math. Geol. 13 (1981) 471–478.
[43] I. Dunkl, TRACKKEY: a Windows program for calculation and graphical presentation of fission track data, Comput. Geosci. 28 (2002) 3–12.
[44] D. York, Least-squares fitting of a straight line with correlated errors, Earth Planet. Sci. Lett. 5 (1969) 320–324.
[45] T.A. Ehlers, K.A. Farley, Apatite (U–Th)/He thermochronometry: methods and applications to problems in tectonic and surface processes, Earth Planet. Sci. Lett. 206 (2003) 1–14.
[46] K. Stüwe, L. White, R. Brown, The influence of eroding topography on steady-state isotherms. Application to fission track analysis, Earth Planet. Sci. Lett. 124 (1994) 63–74.
[47] N.S. Mancktelow, B. Grasemann, Time-dependent effects of heat advection and topography on cooling histories during erosion, Tectonophysics 270 (1997) 167–195.
[48] J. Braun, Quantifying the effect of recent relief changes on age–elevation relationships, Earth Planet. Sci. Lett. 200 (2002) 331–343.
[49] T. Kohl, R.J. Hopkirk, "FRACTure" a simulation code for forced fluid flow and transport in fractured porous rock, Geothermics 24 (3) (1995) 345–359.
[50] T. Kohl, S. Signorelli, L. Rybach, Three-dimensional (3-D) thermal investigation below high Alpine topography, Phys. Earth Planet. Inter. 126 (2001) 195–210.
[51] T.A. Ehlers, T. Chaudhri, S. Kumar, C. Fuller, S. Willett, Ketch, M.T. Brandon, D. Belton, B. Kohn, A.J.W. Gleadow, T. Dunai, F. Fu, Computational tools for low-temperature thermochronometer interpretation, Rev. Mineral. Geochem. 58 (2005) 589–622.
[52] T.A. Ehlers, P.A. Armstrong, D.S. Chapman, Normal fault thermal regimes and the interpretation of low-temperature thermochronometers, Phys. Earth Planet. Inter. 126 (2001) 179–194.
[54] L. Seeber, V. Gornitz, River profiles along the Himalayan arc as indicators of active tectonics, Tectonophysics 92 (1983) 335–367.
[55] M.R. Pandey, R.P. Tandukar, J.P. Avouac, J. Lavé, J.P. Massot, Interseismic strain accumulation on the Himalayan crustal ramp (Nepal), Geophys. Res. Lett. 22 (1995) 751–754.
[56] R. Cattin, J.P. Avouac, Modeling mountain building and the seismic cycle in the Himalaya of Nepal, J. Geophys. Res. 105 (2000) 13389–13407.
[57] R. Bilham, K. Larson, J. Freymuller, P.I. Members, GPS measurements of present-day convergence across the Nepal Himalaya, Nature 386 (1997) 61–64.
[58] D. Whipp, T. Ehlers, A. Blythe, K.W. Huntington, K. Hodges, D. Burbank, Plio–Quaternary Erosion and Kinematic History of the Central Himalaya: thermo-kinematic model of thermochronometer exhumation, Tectonics (in press).
[59] K.V. Hodges, R.R. Parrish, M.P. Searle, Tectonic evolution of the central Annapurna Range, Nepalese Himalayas, Tectonics 15 (1996) 1264–1291.
[60] J.D. Nieman, N.M. Gasparini, G.E. Tucker, R.L. Bras, A quantitative evaluation of Playfair's Law and its use in testing long-term stream erosion models, Earth Surf. Processes Landf. 26 (2001) 1317–1332.
[61] K.X. Whipple, G.E. Tucker, Dynamics of the stream-power river incision model: implications for height limits of mountain ranges, landscape response timescales, and research needs, J. Geophys. Res. 104 (1999) 17661–17674.
[62] A.E. Blythe, D.W. Burbank, A. Carter, K. Schmidt, J. Putkonen, Plio–Quaternary exhumation history of the central Himalaya: 1. Apatite and zircon fission-track and apatite (U–Th)/He analyses, Tectonics (in press).
[63] P.G. Fitzgerald, R.B. Sorkhabi, T.F. Redfield, E. Stump, Uplift and denudation of the central Alaska Range: a case study in the use of apatite fission track thermochronology to determine absolute uplift parameters, J. Geophys. Res. 100 (1995) 20,175–20,191.
[64] M.P. Searle, S.R. Noble, A.J. Hurford, D.C. Rex, Age of crustal melting, emplacement and exhumation history of the Shivling leucogranite, Garhwal Himalaya, Geol. Mag. 136 (1999) 513–525.
[65] D.M. Robinson, P.G. DeCelles, C.N. Garzione, O.N. Pearson, T.M. Harrison, E.J. Catlos, Kinematic model for the Main Central Thrust in Nepal, Geology 31 (2003) 359–362.
[66] M.E. Raymo, The initiation of Northern Hemisphere glaciation, Annu. Rev. Earth Planet. Sci. 22 (1994) 353–383.

[67] M.A. Maslin, X.S. Li, M.-F. Loutre, A. Berger, The contribution of orbital forcing to the progressive intensification of Northern Hemisphere glaciation, Quat. Sci. Rev. 17 (1998) 411–426.
[68] J.C. Zachos, M. Pagani, L. Sloan, E. Thomas, K. Billups, Trends, rhythms, and aberrations in global climate 65 Ma to Present, Science 292 (2001) 686–693.
[69] P. Molnar, Late Cenozoic increase in accumulation rates of terrestrial sediment: how might climate change have affected erosion rates? Annu. Rev. Earth Planet. Sci. 32 (2004) 67–89.
[70] A. Zhisheng, J.E. Kutzbach, W.L. Prell, S.C. Porter, Evolution of Asian monsoons and phased uplift of the Himalaya–Tibetan plateau since Late Miocene times, Nature 411 (2001) 62–66.
[71] X. Quiang, Z. Li, C.M. Powell, H. Zheng, Magnetostratigraphic record of the Late Miocene onset of the East Asian monsoon, and Pliocene uplift of northern Tibet, Earth Planet. Sci. Lett. 187 (2001) 83–93.
[72] A.K. Gupta, E. Thomas, Initiation of Northern Hemisphere glaciation and strengthening of the northeast Indian monsoon: Ocean Drilling Program Site 758, eastern equatorial Indian Ocean, Geology 31 (2003) 47–50.
[73] D.W. Burbank, L. Derry, C. France-Lanord, Lower Himalayan detrital sediment delivery despite an intensified monsoon at 8 Ma, Nature 364 (1993) 48–50.
[74] P.D. Clift, A. Carter, M. Krol, E. Kirby, Constraints on India–Eurasia collision in the Arabian Sea region taken from the Indus Group, Ladakh Himalaya, India, in: P.D. Clift, D. Kroon, C. Gaedicke, J. Craig (Eds.), The Tectonic and Climatic Evolution of the Arabian Sea Region, Geological Society of London Special Publication, vol. 195, Goelogical Society of London, London, 2002, pp. 97–116.
[75] F. Metivier, Y. Gaudemer, P. Tapponier, M. Klein, Mass accumulation rates in Asia during the Cenozoic, Geophys. J. Int. 137 (1999) 280–318.
[76] P. Clift, G. Layne, J. Blusztajn, The erosional record of Tibetan uplift in the East Asian marginal seas, in: P. Clift, P. Wang, D. Hayes, W. Kuhnt (Eds.), Continent–Ocean Interactions in the East Asian Marginal Seas, American Geophysical Union, 2004, monograph.
[77] P. Zhang, P. Molnar, W. Downs, Increased sedimentation rates and grain sizes 2–4 Myr ago due to the influence of climate change on erosion rates, Nature 410 (2001) 891–897.
[78] C. Wobus, K. Hodges, K. Whipple, Topographic signatures of neotectonics in the central Nepal Himalaya, Eos, Trans. - AGU 84 (2003) (Fall Meet. Suppl., Abstract T21C-0469).
[79] M. Colchen, P. LeFort, A. Pêcher, Annapurna-Manaslu-Ganesh Himal, Centre National de la Recherche Scientifique, Paris, 1986, 136 pp.
[80] A. Pêcher, The metamorphism in the central Himalaya, J. Metamorph. Geol. 7 (1989) 31–41.
[81] A.L. Martin, P.G. DeCelles, G.E. Gehrels, P.J. Patchett, C. Isachsen, Isotopic and structural constraints on the location of the Main Central thrust in the Annapurna Range, central Nepal Himalaya, Geol. Soc. Amer. Bull. 117 (2005) 926–944.
[82] P.W. Reiners, Zircon (U–Th)/He thermochronometry, Rev. Mineral. Geochem. 58 (2005) 151–179.

References cited in Appendix B

[1] T.A. Ehlers, P.A. Armstrong, D.S. Chapman, Normal fault thermal regimes and the interpretation of low-temperature thermochronometers, Phys. Earth Planet. Inter. 126 (2001) 179–194.
[2] D. Whipp, T. Ehlers, A. Blythe, K.W. Huntington, K. Hodges, D. Burbank, Plio–Quaternary Erosion and Kinematic History of the Central Himalaya: thermo-kinematic model of thermochronometer exhumation, Tectonics (in press).
[3] J.P. Platt, J.I. Soto, M.C. Comas, L.S. Scientists, Decompression and high-temperature–low-pressure metamorphism in the exhumed floor of an extensional basin, Alboran Sea, western Mediterranean, Geology 24 (1996) 447–450.
[4] K. Hodges, C. Wobus, K. Ruhl, T. Schildgen, K. Whipple, Quaternary deformation, river steepening, and heavy precipitation at the front of the Higher Himalayan ranges, Earth Planet. Sci. Lett. 220 (2004) 379–389.
[5] T. Kohl, R.J. Hopkirk, "FRACTure" a simulation code for forced fluid flow and transport in fractured porous rock, Geothermics 24 (3) (1995) 345–359.
[6] T. Kohl, S. Signorelli, L. Rybach, Three-dimensional (3-D) thermal investigation below high Alpine topography, Phys. Earth Planet. Inter. 126 (2001) 195–210.
[7] P. Henry, X. Le Pichon, B. Goffé, Kinematic, thermal and petrologic model of the Himalayas: constraints related to metamorphism within the underthrust Indian crust and topographic elevation, Tectonophysics 273 (1997) 31–56.
[8] F.D. Hansen, N.L. Carter, Creep of selected crustal rocks at 1000 MPa, Trans. Am. Geophys. Union 63 (1982) 437.
[9] T.A. Ehlers, T. Chaudhri, S. Kumar, C. Fuller, S. Willett, Ketch, M.T. Brandon, D. Belton, B. Kohn, A.J.W. Gleadow, T. Dunai, F. Fu, Computational tools for low-temperature thermochronometer interpretation, Rev. Mineral. Geochem. 58 (2005) 589–622.